Papers in Physics, vol. 15, art. 150004 (2023)

www.papersinphysics.org

Received: 29 March 2023, Accepted: 09 September 2023
Edited by: O. Fojón

DOI: https://doi.org/10.4279/PIP.150004

ISSN 1852-4249

Insights into vibrational and electronic properties of (6,6)-phenyl-C61-butyric acid methyl ester (PCBM) chemical bonding with $(CuO)_n$ clusters: a DFT study

C E Martinez-Nuñez[1]*, Y Delgado-Beleño[1], M Cortez-Valadez[2], O Rocha-Rocha[1], Ramón A B Alvarez [1], M Flores-Acosta[2]

Density functional theory (DFT) was used to study the electronic and vibrational properties of the chemical bond between the [6,6]-phenyl-C61-Butyric acid methyl ester (PCBM) and $(CuO)_n$ clusters. After chemical adsorption, the HOMO orbitals of PCBM primarily shifted towards $(CuO)_n$, leading to a noticeable reduction in the band gap. Similarly, the bond established is responsible for the spatial redistribution of boundary orbitals, mainly towards the clusters. In addition, the orbital analysis revealed that the primary contributions to the chemical bond originated from the Cu atoms. The PCBM Raman intensity shows a meaningful enhancement consequence of the chemical bond established with the clusters. In addition, new normal modes of PCBM are observed in the Raman activity spectrum after the chemical adsorption.

I Introduction

Experiments carried out by Kroto et al. led to the discovery of a special type of fullerene known as buckminsterfullerene, C_{60} [1, 2]. Consequently, several experimental and theoretical investigations have been realized to determine its geometrical, chemical, physical, and biological properties, among others [3–5]. The inherent properties of C_{60} have been used to develop a great number of applications in different fields of science [6]. Recent reports show some fullerenes' derivatives exhibit outstanding biological properties, such as antioxidant and antibacterial, as a consequence, and have been used in therapies for conditions such as osteoporosis and HIV, among others [7, 8]. Similarly, studies have been carried out on the development of renewable energies [9, 10]. Among the C_{60} derivatives, the [6,6]-phenyl-C61-Butyric acid methyl ester, PCBM, [11] has been used to synthesize efficient organic solar cells, nano biological devices, and other applications due to its thermal and optical properties [12–17]. Additionally, theoretical research using the density functional theory, DFT, and time-dependent density functional theory, TD-DFT, [18] has been employed to study the optical and vibrational properties of PCBM and its complexes [19, 20]. Additionally, Surface Enhanced Raman Spectroscopy (SERS) studies have been made to analyze the PCBM vibrational properties using gold nanoparticles, AuNPs [21]. The intraband and interband electron transition consequence of the surface plasmon resonance, SPR, of AuNPs was studied using the DFT. In same way, studies of the SERS effect complexes of PCBM with silver nano-prisms have been made for solar cell

* ceduardomartinez@unicesar.edu.co

[1] Universidad Popular del Cesar, 200003 Valledupar, Colombia.

[2] Universidad de Sonora, Hermosillo 83000, México.

applications [22]. The overall contribution to the SERS effect in the later research was attributed to the active SPR of the silver nano-prisms. Other SERS mechanisms using semiconductor nanoparticles have been used to study the vibrational properties of PCBM experimentally and theoretically [23, 24]. The chemical bonding mechanism, CB, was considered to explain the overall contribution to the SERS effect by the presence of semiconductor nanoparticles employing the DFT. However, the underlying properties of CB continue to be a research interest. This work considers some underlying properties of the chemical bonding mechanism between PCBM and copper oxide clusters, $(CuO)_n$, n = 2, 4 and 6. Accordingly, the DFT calculations were carried out to study the electronic and vibrational properties of the complex PCBM-$(CuO)_n$. The CB mechanism is studied as the main contribution to the SERS effect of PCBM, consequence of the bond established with $(CuO)_n$ clusters.

II Computational methods

The structure of C_{60} was made with the advanced molecule editor and visualizer software Avogadro following the Schlegel diagrams [5, 25]. Then, the ligand phenyl and butyric acid methyl ester (PBM) were placed between two 6-membered rings of C_{60} [6,6], and the $(CuO)_n$ clusters were located opposite the PBM and near a 6-membered ring of C_{60}. The calculations were performed in gas phase and the alignment of $(CuO)_n$ respect to PCBM molecule math the default x-axis of GaussView software. The geometric optimization and vibrational calculations were carried out with the commercial software Gaussian 09 [26], using the theory level DFT [27], the hybrid B3LYP functional [28], and the LanL2DZ basis set [29–31]. The Gaussian output files were analyzed using the software Multifunctional Wavefunction Analyzer (Multiwfn) [32]. The orbital composition analysis was carried out using the Mulliken population method [33] implemented in Multiwfn. Similarly, the Hirshfeld population analysis [34–36] was used to perform the orbital study [37]. In contrast, all the isosurfaces presented in this work were rendered using the molecular visualization software Visual Molecular Dynamics (VMD) [38].

With the purpose of comparing the Raman intensity of PCBM before and after the chemical adsorption of $(CuO)_n$ clusters, the integral Raman enhancement, EF_{int}, was used [39]. This quantity is defined in terms of the ratio of total Raman cross-section of the complex PCBM-$(CuO)_n$, $I^{total}_{PCBM\text{-}(CuO)_n}$, and the free PCBM structure, I^{total}_{PCBM}. In consequence, EF_{int} is given by [39]:

$$EF_{int} = \frac{I^{total}_{PCBM\text{-}(CuO)_n}}{I^{total}_{PCBM}} = \frac{\sum_k I^k_{PCBM\text{-}(CuO)_n}}{\sum_j I^j_{PCBM}} \quad (1)$$

where $I^k_{PCBM\text{-}(CuO)_n}$ and I^j_{PCBM} are the differential Raman cross-section of the k^{th} and j_{th} normal modes of the PCBM-$(CuO)_n$ complex and PCBM, respectively.

The bond properties between the PCBM and $(CuO)_n$ was determined using the potential energy density, V(r), the gradient kinetic energy density, G(r), and the total electronic energy density, H(r), at the bonding critical point, defined as [40]:

$$H(r) = V(r) + G(r) \quad (2)$$

where H(r) is negative for interactions with significant sharing of electrons and reflects the covalent character of the interaction [41]. V(r) and G(r) are related with the electron density, ρ(r), for a stationary state as follows [40]:

$$\left(\frac{\hbar^2}{4m}\right)\nabla^2\rho(r) = 2G(r) + V(r) \quad (3)$$

The dimensionless $|V(r)|/G(r)$ ratio is commonly used to determine the characteristic bonding regime [42]. When $|V(r)|/G(r) > 1$, this gives evidence of relatively stable bonding dominated by the potential energy [43].

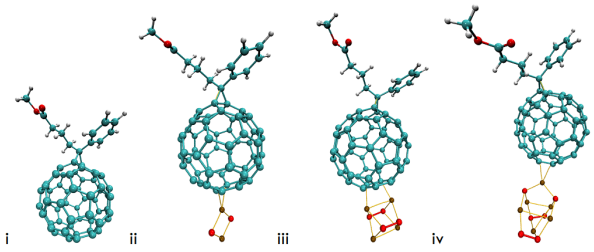

Figure 1: Optimized geometry of PCBM and PCBM-$(CuO)_n$ complexes obtained with DFT.

III Results

i Orbital analysis

The electronic properties of the complex PCBM-$(CuO)_n$, could be affected by the starting geometry; in consequence, the optimization was made according to the configuration proposed by N. Van den Brande et al. [20]. This means the $(CuO)_n$ clusters were oriented to the opposite side of the functional group PBM and place at [6,6] type C-C bond, coinciding with the Ricardo Pino-Rios et al. study [44], which indicates this bond shows a higher tendency for electrophilic attack and consequently reacts by forming strong bonds.

The optimized geometries of PCBM and PCBM-$(CuO)_n$, n = 2, 4 and 6, were obtained using the DFT calculations (see Fig. 1). To analyze the spatial distribution before and after the chemical adsorption of the $(CuO)_n$ clusters, the highest and lowest occupied molecular orbital, HOMO and LUMO, of PCBM and PCBM-$(CuO)_n$ were used (see Fig. 2). The HOMO and LUMO of PCBM are meanly located at C_{60} with an energy level of -6.3 and -3.7 eV, respectively. After the chemical adsorption, HOMO is mostly distributed at $(CuO)_n$ clusters. Specifically, the distribution of HOMO and LUMO in PCBM-$(CuO)_4$ exhibits significant distinctions when compared to the other complexes (see Fig. 2). This distinction arises due to the chemical adsorption of $(CuO)_4$, where two bonds were formed between distinct carbon, C, and copper, Cu, atoms. This process contrasts with the method employed for the other clusters (see Fig. 1). However, Fig. 3 demonstrates a significant shift in the energy levels of HOMO and LUMO, along with a substantial reduction in the band gap, GAP, consequence of CB established with the clusters. The case of PCBM -$(CuO)_4$ shows an energy shift of HOMO and LUMO towards higher values, this behavior being a consequence of the cluster chemical adsorption as previously described. The reduction and the energy shift of PCBM orbitals due to the effects of chemical interactions have been similarly reported by N. Van den Brande et al. [20].

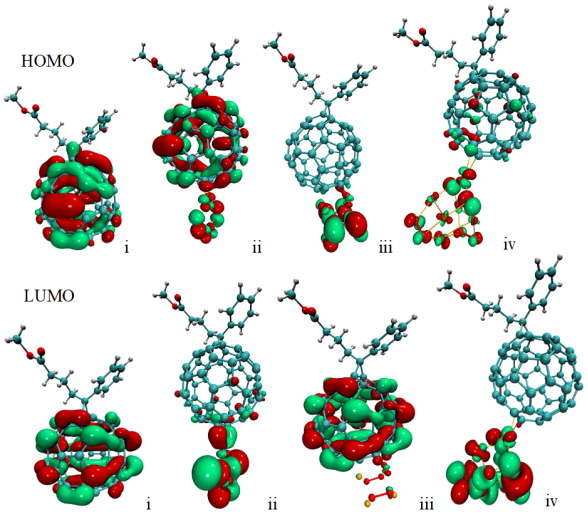

Figure 2: HOMO and LUMO orbitals i) PCBM and ii-iv) PCBM-$(CuO)_n$, n = 2, 4 and 6

To study the effects of an external electric field over the electronic and vibrational properties of PCBM-$(CuO)_4$ complex, an electric dipole field, E_x, of magnitude 0.001 u.a. was applied in calculation. This complex was selected because it shows the HOMO highly distributed at cluster regions (see Fig. 2-iii). The electrostatic potential surface, EPS, was taken to visualize the charge density before and after the application of E_x. The red and orange regions correspond to higher electron density and the blue region to lower. The calculation reveals major contributions of $(CuO)_4$ to HOMO as described before; however, a significant quantity of electron density is observed at the C_{60} region (see SI-Fig.1-i and 1-ii in Supporting Information (SI)). The HOMO and LUMO energy levels were raised to higher values of -4.2 and -3.97 eV, respectively. The energy gap was significantly reduced to 0.23 eV compared to the calculation results obtained prior to E_x application (see Fig. 3). Additionally, a sig-

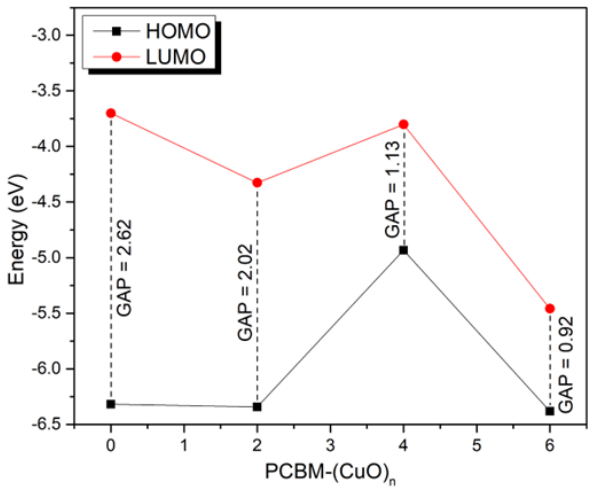

Figure 3: Gap HOMO-LUMO of PCBM and PCBM-$(CuO)_n$, n = 2, 4 and 6

nificant part of the HOMO isosurface is located at the PCBM region, and the LUMO isosurface is redistributed to the PBM ligand (see SI-Fig.1-iii).

Figure 4 shows the critical points, CPs, of the complexes PCBM-$(CuO)_n$, n = 4, 6. These CPs correspond to the spatial points where the gradient of electron density, $\rho(r)$, vanishes, which means $\Delta\rho(r) = 0$ [40]. The CPs were used to study the orbital properties between PCBM and $(CuO)_n$, n = 4, 6 clusters. The CP between the bonds Cu-C involved in the CB corresponds to a bond critical point, BCP, and the CP inner (3, 4)-membered Cu-C ring is known as ring critical point, RCP, [37,40].

Table 1: Energy density parameters at BCPs. Where CP, ρ(r), V(r), G(r) and H(r) correspond to critical point, electronic, potential, kinetic and total energy density, respectively. Units are a.u.

PC	ρ(r)	V(r)	G(r)	H(r)	|V(r)|/G(r)
PCBM-$(CuO)_4$					
BPC1	0.27	−0.09	0.07	−0.006	1.08
BPC2	0.28	−0.08	0.08	−0.007	1.09
PCBM-$(CuO)_6$					
BPC1	0.29	−0.08	0.06	−0.004	1.05
BPC2	0.28	−0.08	0.07	−0.005	1.07

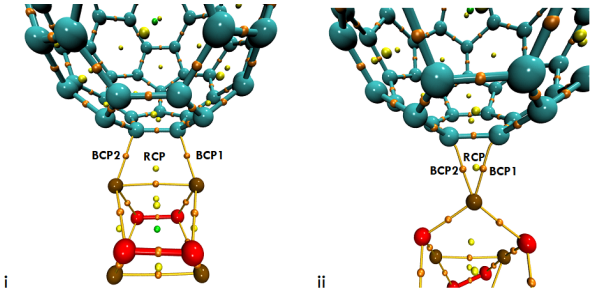

Figure 4: Electrostatic potential surface (EPS) of HOMO and LUMO orbitals of PCBM and the complexes PCBM-$(CuO)_n$, n = 4, 6.

The BCPs with $\rho(r) > 0.2$ au and the negative sign of H(r) indicate the presence of a shared covalent bond [40, 41]. The values of $\rho(r)$ from the BCP1 and BCP2 related to the bonds between PCBM and $(CuO)_4$ cluster correspond to 0.27 and 0.28

Table 2: Occupied Orbitals contributions to bond critical points (BCPs) and Ring critical points (RCP) of a) PCBM-(CuO)4 and b) PCBM-(CuO)6

CP	Orb.	E (eV)	%*	CuO (%)†
PCBM-$(CuO)_4$				
BPC1	HOMO - 55	−10.2	70	20.2
	HOMO - 39	−9.02	11	85.6
BPC2	HOMO - 110	−13.6	67	17.3
	HOMO - 36	−8.7	13	88.3
RPC	HOMO - 55	−10.2	18	20.2
	HOMO - 40	−9.07	16	98.3
	HOMO - 41	−9.12	16	98.2
	HOMO - 110	−13.6	14	17.3
PCBM-$(CuO)_6$				
BPC1	HOMO - 125	−13.62	48.5	14.2
	HOMO - 17	−7.84	16.4	95.5
	HOMO - 125	−7.82	11.5	80.8
BPC2	HOMO - 110	- - -	- - -	- - -
	HOMO - 17	- - -	- - -	- - -
	HOMO - 15	- - -	- - -	- - -
RPC	HOMO - 125	- - -	- - -	- - -
	HOMO - 17	- - -	- - -	- - -
	HOMO - 175	−21.76	12.6	1.75

Contribution from occupied orbitals of PCBM-$(CuO)_n$ complex (*) and $(CuO)_n$ cluster (†).

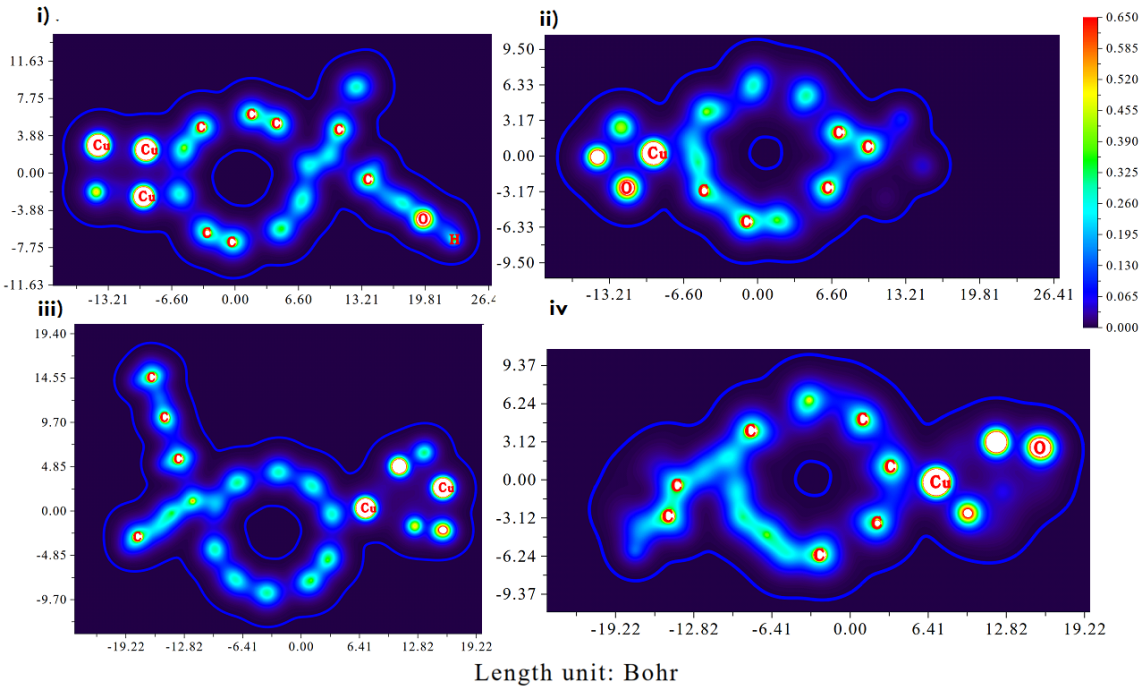

Figure 5: Color-filled map of electron density of: i-ii) Planes XY (Z = 0.2 Borh) and YZ (Y = 2.0 Bohr) of PCBM-$(CuO)_4$, respectively; and iii-iv) Planes XY (Z = 0.2 Borh) and YZ (Y = 0.2 Bohr) of PCBM-$(CuO)_6$, respectively.

a.u (see Table 1). For both BCPs, H(r) is negative and $|V(r)|/G(r) > 1$, which means the chemical bond Cu-C corresponds to a covalent bond. Similar behavior is observed for the bond character of PCBM-$(CuO)_6$ complex. Table 2 shows the orbital contributions of $(CuO)_n$ clusters to BCPs and RCPs. The occupied orbitals with higher contributions to BCP1 and BCP2 of the complex PCBM-$(CuO)_4$ came from the orbitals HOMO - 55 (70%) and HOMO - 110 (67%) with energy levels −10.2 and −13.6 eV respectively. The charge contribution from $(CuO)_4$ to these orbitals corresponds to 20.2 and 17.3% respectively. On the other hand, the orbitals HOMO - 39 and HOMO - 36 manifest the lower charge contributions to BCPs, corresponding to 11 and 13% respectively. However, the $(CuO)_4$ cluster exhibits the higher charge contributions to these orbitals. The case of RCP evidences a different behavior; despite the fact charge contribution from occupied orbitals is lower ∼16%, the calculate $\rho(r)$ have a similar magnitude to BCPs, 0.23 a.u., even though the charge contribution from $(CuO)_4$ is higher. With respect to the PCBM-$(CuO)_6$ complex, the major occupied orbital contributions to BCP1 and BCP2 came from the orbitals HOMO - 125 (48.5%) and HOMO - 17 (16.4%) with energy levels −13.62 and −7.84 eV respectively. The $(CuO)_6$ cluster contributes 14.2% and 95.5% to these orbitals, respectively, showcasing distinct behavior compared to the $(CuO)_4$ cluster. The orbitals with higher contributions to BCPs from the $(CuO)_4$ and $(CuO)_6$ clusters are shown in SI-Fig.2 and SI-Fig.3. Fig. 5-i and 5-ii, show the color-filled map of PCBM-$(CuO)_4$ electron density in the planes X-Y (Z = 0.2 Bohr) and X-Z (Y = 2.0 Bohr), respectively. The figures illustrate a meaningful $\rho(r)$ of the covalent bond Cu-C described in the BCPs analysis. Similar behavior is observed in the covalent bond between PCBM and the $(CuO)_6$ (see Fig. 5-iii and 5-iv).

To obtain a clear illustration of the boundary orbital contributions to CB from the $(CuO)_n$ clusters, the discrete energy levels of the PCBM-$(CuO)_n$ complexes were broadened using normal-

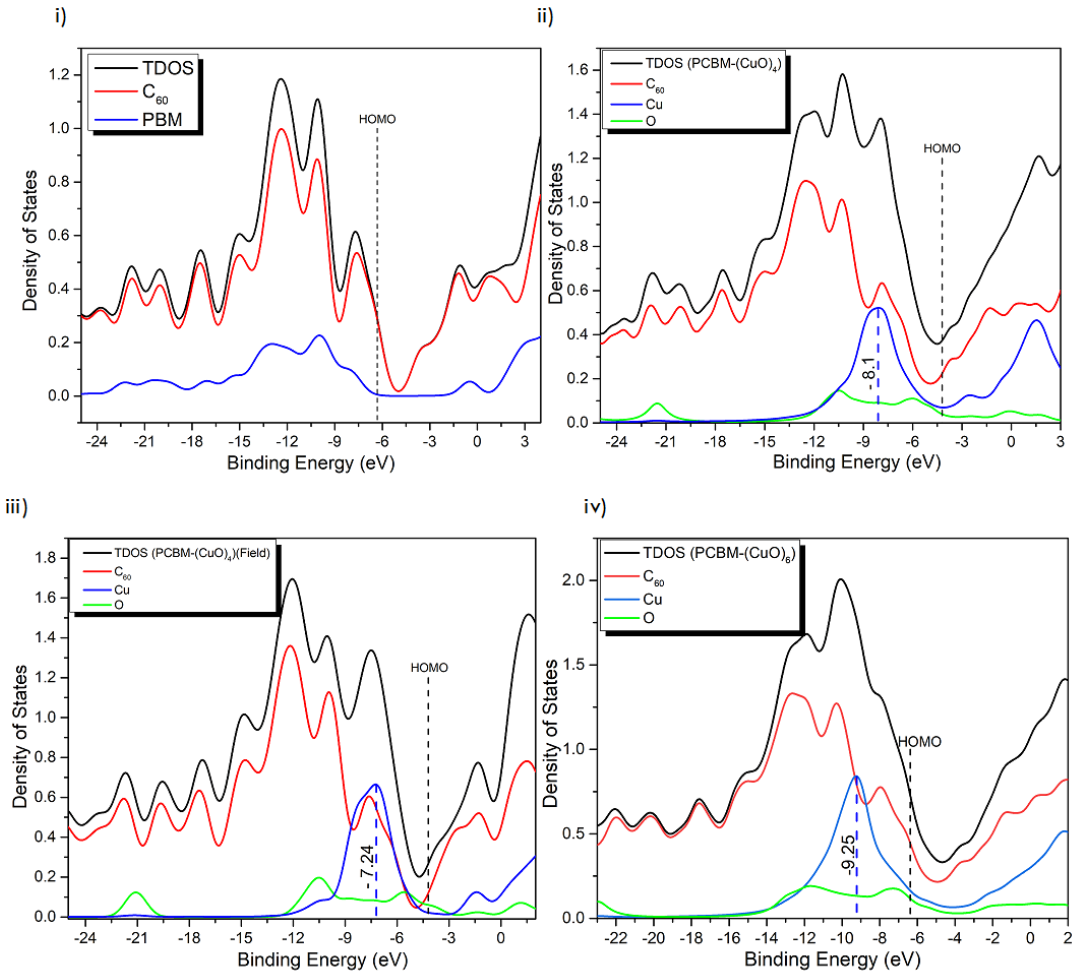

Figure 6: Total and partial density of states (TDOS and PDOS) of i) PCBM, ii) PCBM-$(CuO)_4$, iii) PCBM-$(CuO)_4$+E_x, iv) PCBM-$(CuO)_6$

ized Lorentzian functions. Consequently, the density of states (DOS) was obtained to analyze its electronic structure. Fig. 6-i shows the total density of states (TDOS) of PCBM and the partial density of states (PDOS) of C_{60} and the ligand PBM. Vertical dash line indicates the HOMO energy level. The figure exhibits overall contribution to the boundary orbitals from C_{60}, whereas the contribution from PBM is meaningless, as described by Cairong Zhang et al. [18]. After the chemical adsorption of the $(CuO)_4$ cluster, the PDOS reveals a collective contribution to the TDOS originating primarily from C_{60} orbitals. Nonetheless, the $(CuO)_4$ cluster exhibits a notable impact on the boundary orbitals, particularly attributable to the presence of Cu atoms (see Fig. 6-ii). This fact aligns with the energy reordering as detailed by N. Van den Brande et al. [20]. The peak centered at −8.1 eV corresponds to the PDOS of Cu atoms encompassing the occupied orbitals ranging HOMO – 41 to HOMO - 39 and HOMO - 36 with energy levels between −14 and −6 eV. These orbitals have the main charge contributions to BCPs and RCP, as described before in the CPs analysis (Table 2). Fig. 6-iii reveals the TDOS of PCBM-$(CuO)_4$ under the action of E_x. The PDOS indicates an increase

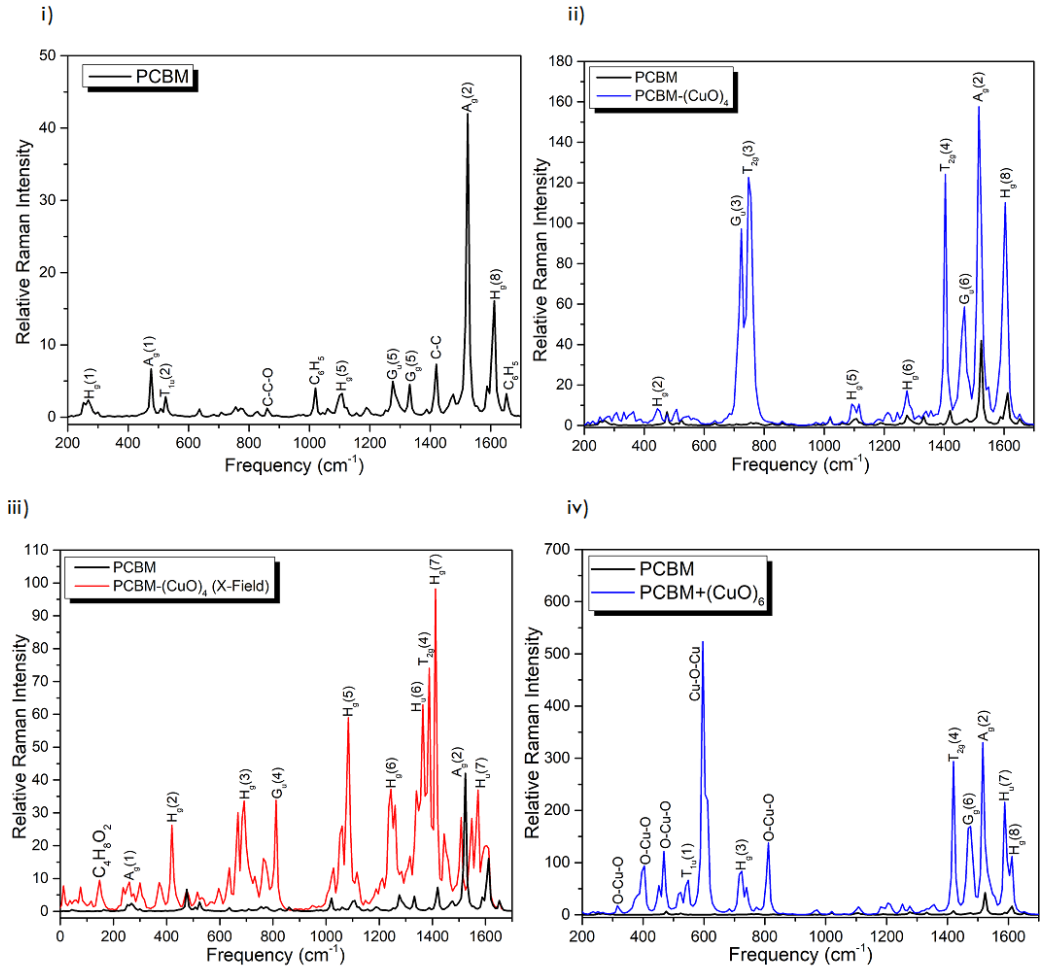

Figure 7: Raman intensity spectrum of the vibrational modes of i) PCBM, ii) PCBM-$(CuO)_4$, iii) PCBM-$(CuO)_4$+E_x, iv) PCBM-$(CuO)_6$

of the contribution to $(CuO)_4$ cluster to BCPs orbitals, mainly from the Cu atoms. Furthermore, an increase is observed in the orbital contribution of oxygen atoms to the HOMO from the $(CuO)_4$ cluster, attributed to the effect of E_x. The peak with a maximum at −7.24 eV encompasses orbitals ranging in energy levels from −12 to −5 eV, involving the occupied orbitals with higher contributions to BCPs. Similar behavior in TDOS and PDOS is observed in PCBM-$(CuO)_6$ (see Fig. 6-iv), however, due to the CB established, there is an observable downward shift in the HOMO energy level to −6.38 eV, closely resembling the HOMO energy level of PCBM prior to chemical adsorption. The Peak at −9.25 eV encompasses the set of orbitals involved in CB with a significant charge contribution from Cu atoms of the $(CuO)_6$ cluster.

ii Raman activity analysis

Fig. 7-i shows the Raman activity spectrum of the PCBM vibrational modes. Most of the modes were assigned to C_{60} according the nomenclature proposed by Weeks and Harter [45–47] based on the irreducible representation labels of each vibrational mode. For example, the radial vibrational mode, or breathing mode, of C_{60} is labelled as A_g mode.

The frequency, Raman intensity, and the vibration type of PCBM corresponding to this work, the theoretical and experimental results reported by H. Kuzmany et al. and V. Schettino [48,49] are presented in SI-Table 2-i. The vibrational spectrum is characterized by two intense modes, one $A_g(2)$ at 1523.3 cm^{-1}, and the other $H_g(8)$ at 1609.9 cm^{-1} as previously described by Cairong Zhang [18]. Other modes with less intensities correspond to $H_g(1)$, $A_g(1)$ and $T_{1u}(2)$ in the frecuency range of $200-600$ cm^{-1}, characteristic modes of the phenyl and butyric acid groups, C-C-O and C_6H_5, in the range $800-1050$ cm^{-1}, the modes $H^g(5)$, $G_u(5)$ and $G_g(5)$ in the range $1050-1400$ cm^{-1} and the $C-C$ vibrational mode of the ligand to fullerene bond at 1417 cm^{-1}. Most of the vibrational modes described above show a shift compared to the experimental and theoretical reports, possibly by the coupling ligand to fullerene. The Raman activity after the chemical adsorption of the$(CuO)_n$ cluster is observed in Fig. 7-ii. The Raman lines correspond mainly to C_{60} vibrational modes and show the same shift consequence of the coupling to phenyl group and the clusters [18]. Overall the spectrum shows meaningful enhancements, especially the modes $A_g(2)$, $H_g(8)$, and the inactive modes $G_u(3)$ and $T_{2g}(3)$ in the range $600-800$ cm^{-1}, $T_{2g}(4)$ and $G_u(6)$ in the range $1350-1500$ cm^{-1} due to the CB established (see SI-Table 2-ii). The vibrational modes attributed to the phenyl group and the C-C bond, ligand to fullerene, do not exhibit notable intensities. The Raman activity of the PCBM-$(CuO)_4$ complex after applying E_x is shown in Fig. 7-iii. The vibrational spectrum is dominated mainly by enhancements of the modes $H_g(2)$, $H_g(3)$, $G_u(2)$, $H_g(5)$, $H_g(6)$, $H_u(6)$, $T_{2g}(4)$, $H_g(7)$ and $H_u(7)$ some of then inactive after E_x (see SI-Table 2-iii). The higher enhancements of PCBM Raman lines were obtained by the presence of the $(CuO)_6$ cluster, especially the modes in range $1400-1600$ cm^{-1}. The stretching and bending modes of O-Cu-O and Cu-O-Cu are also significant in the overall spectrum (see Fig. 7-iv and SI-Table 2-iv).

Table 3 presents the integrated Raman enhancement, EF_{int}, values calculated from the PCBM-$(CuO)_n$ complex in comparison to the isolated PCBM molecule. The obtained values of EF_{int} vary from 2.03 for the smallest cluster to 18.16 for the largest. EF_{int} from PCBM-$(CuO)_4$ has similar value before and after applying the E_x, this means the contributions to overall enhancements may come mainly from the CB established rather than the effects of an external field, besides the meaningful charge distribution observed at PCBM in the complex (Fig. 3-iv). The author Zhao et al., reported EF_{int} values from 2.54 to 5.83 of silver clusters, Ag_6 and Ag_8, chemically adsorbed at the organic molecule Pyridine, Py [50,51]. Higher values of 8.65 were obtained for bigger cluster such as Ag_{20} and Ag_{68} [50, 51]. Additionally, the overall contribution to the Raman enhancement was reported due to the energy difference between the HOMO of the cluster and the LUMO of the molecule, rather than the amount of charge transferred. In this sense, we suppose the contribution to the overall enhancement of PCBM is mainly a consequence of the effects of the CB established with the $(CuO)_n$ cluster due to the HOMO of PCBM-$(CuO)_n$ complexes being mainly located to $(CuO)_n$ regions and the LUMO being mainly distributed to the PCBM region. Additionally, a significant reduction of energy gap was observed.

Table 3: Integral Raman enhancement, EF_{int}, calculations of the complexes PCBM-$(CuO)_n$, n = 2, 4, and 6 concerning the PCBM Raman intensity.

Complex	EF_{int}
PCBM-$(CuO)_2$	2.03
PCBM-$(CuO)_4$	7.13
PCBM-$(CuO)_4$+E_x	7.76
PCBM-$(CuO)_6$	18.16

IV Conclusions

We obtain relevant electronic and vibrational properties of PCBM and the complexes PCBM-$(CuO)_n$ using the DFT calculations. Calculated Raman spectrum of PCBM is characterized by C_{60} vibrational modes affected for the coupling with phenyl and butyric acid groups and the presence of $(CuO)_n$ clusters. Intensity enhancements of PCBM vibrational modes were observed because of the chemical bond established with $(CuO)_n$ clusters. Additionally, new normal modes in the Raman lines

spectrum of PCBM were identified after the chemical adsorption of the clusters. Spatial distribution of HOMO is mainly observed at $(CuO)_n$ clusters before the chemical adsorption. CPs, DOS and PDOS studies reveal the major electronic contribution of $(CuO)_n$ at CB came from the boundary orbitals, especially from the Cu atoms. Action of an electric dipole field in x-direction does not produce significant increases, but was, however, useful to stimulate certain vibrational modes of PCBM, as for instance the Hg family modes. The integrated Raman enhancement values obtained from PCBM-$(CuO)_n$ complexes were significant considering other studies like the interaction of Ag cluster with Py molecule. The overall contribution to the increase of PCBM Raman lines is attributed to the effects of CB mechanism established with $(CuO)_n$ clusters.

Acknowledgements - This work was supported by A1-S-46242 project of the CONAHCYT Basic Science. The author M. Cortez-Valadez appreciates the support by "Investigadores por México" program. We are grateful for the support through the High-Performance Computing Area of the University of Sonora (ACARUS).

[1] H. W. Kroto, J. R. Heath, S. C. O'Brien, et al., *C60: Buckminsterfullerene*, Nature, **318**, 162, (1985).

[2] H. W. Kroto, A. W. Allaf, S. P. Balm, *C60: Buckminsterfullerene*, Chem. Rev., **91**, 1213, (1991).

[3] S. L. Ren et al., *Ellipsometric determination of the optical constants of C60 (Buckminsterfullerene) films*, Appl. Phys. Lett., **59**, 2678, (1991).

[4] A. Rosén, B. Wästberg, *Buckminsterfullerene C60 a surface with curvature and interesting properties*, Surf Sci, **269**, 1121, (1992).

[5] S. Schein, M. Sands-Kidner, *A geometric principle may guide self-assembly of fullerene cages from clathrin triskelia and from carbon atoms*, Biophys. J., **94**, 958, (2008).

[6] F. Wudl, *The Chemical Properties of Buckminsterfullerene (C60) and the Birth and Infancy of Fulleroids*, Acc. Chem. Res., **25**, 157, (1992).

[7] S. Bosi, et al., *Fullerene derivatives: An attractive tool for biological applications*, Eur. J Med. Chem., **38**, 913, (2003).

[8] T. Da Ros, M. Prato, *Medicinal chemistry with fullerenes and fullerene derivatives*, Chem. Comm., 663, (1999).

[9] M. Notarianni, et al., *Synthesis and applications of carbon nanomaterials for energy generation and storage*, Beilstein J. Nanotech., **7**, 149, (2016).

[10] D. Kronholm, J. C. Hummelen, *Fullerene-based n-type semiconductors in organic electronics.*, Material Matters (Milwaukee, WI, United States), **2**, 16, (2007).

[11] J. C. Hummelen, et al., *Preparation and Characterization of Fulleroid and Methanofullerene Derivatives*, J. Organic Chem., **60**, 532, (1995).

[12] K. Akaike, et al., *Ultraviolet photoelectron spectroscopy and inverse photoemission spectroscopy of [6,6]-phenyl-C61-butyric acid methy ester in gas and solid phases*, J. Appl. Phys., **104**, 023710, (2008).

[13] J. H. Pöhls, M. B. Johnson, M. A. White, *Origins of ultralow thermal conductivity in bulk [6,6]-phenyl-C61-butyric acid methyl ester (PCBM)*, Physical Chemistry Chemical Physics, **18**, 1185, (2016).

[14] J. L. Wu, et al., *Near-infrared laser-driven polymer photovoltaic devices and their biomedical applications*, Energy Environ. Sci., **4**, 3374, (2011).

[15] S. Foster, et al., *Electron collection as a limit to polymer:PCBM solar cell efficiency: Effect of blend microstructure on carrier mobility and device performance in PTB7:PCBM*, Adv. Energy Mater, **4**, 1, (2014).

[16] J. Guo, et al., *Structure, dynamics, and power conversion efficiency correlations in a new low*

bandgap polymer: PCBM solar cell, J. Phys. Chem. B, **114**, 742, (2010).

[17] C. H. Chiang, C. G. Wu, *Bulk heterojunction perovskite-PCBM solar cells with high fill factor*, Nat. Photonics, **10**, 196, (2016).

[18] C. Zhang, et al., *DFT Study on Methanofullerene Derivative [6,6]-Phenyl-C61 Butyric Acid Methyl Ester*, Acta Physico - Chimica Sinica, **24**, 1353, (2008).

[19] J. P. Martínez, M. Solà, *Open-Circuit Voltage of Organic Photovoltaics: A Time-Dependent and Unrestricted DFT Study in a P3HT/PCBM Complex*, J. Phys. Chem. A, **124**, 1300, (2020).

[20] N. Van Den Brande, et al., *A time dependent DFT study of the efficiency of polymers for organic photovoltaics at the interface with PCBM*, RSC Adv., **4**, 52658, (2014).

[21] Y. Wu, et al., *SERS Study of the Mechanism of Plasmon-Driven Hot Electron Transfer between Gold Nanoparticles and PCBM*, J. Phys. Chem. C, **123**, 29908, (2019).

[22] M. Stavytska-Barba, et al., *Plasmonic enhancement of Raman scattering from the organic solar cell material P3HT/PCBM by triangular silver nanoprisms* J. Phys. Chem. C, **115**, 20788, (2011).

[23] C. E. Martinez Nuñez, et al., *Chemical bonding mechanism in SERS effect of pyridine by CuO nanoparticles*, J. Raman Spectroscopy, **50**, 1395, (2019).

[24] C. E. Martinez-Nuñez, et al., *Non-resonant enhancement mechanism in SERS effect due to copper oxide quantum dots stabilized in synthetic zeolite F9-NaX*, Mater. Chem. Phys., **211**, 150, (2018).

[25] R. Hoppe, J. Köhler, *SCHLEGEL projections and SCHLEGEL diagrams—new ways to describe and discuss solid state compounds*, Zeitschrift fur Kristallographie - New Crystal Structures, **183**, 77, (1988).

[26] M. J. Frisch et al., *Gaussian 09, Revision D. 01, Gaussian Inc.*, Wallingford, CT, USA (2009).

[27] I. N. Levine, D. H. Busch, H. Shull, *Quantum chemistry*, Prentice Hall Upper Saddle River, NJ, (2000).

[28] A. D. Becke, *Density-functional thermochemistry. III. The role of exact exchange*, J Chem. Phys., **98**, 5648, (1993).

[29] P. J. Hay, *Gaussian basis sets for molecular calculations. The representation of 3d orbitals in transition-metal atoms*, J Chem. Phys., **66**, 4377, (1977).

[30] P. J. Hay, W. R. Wadt, *Ab initio effective core potentials for molecular calculations. Potentials for the transition metal atoms Sc to Hg*, J Chem. Phys., **82**, 270, (1985).

[31] W. R. Wadt, P. J. Hay, *Ab initio effective core potentials for molecular calculations. Potentials for main group elements Na to Bi*, J Chem. Phys., **82**, 284, (1985).

[32] T. Lu, F. Chen, *Multiwfn: A multifunctional wavefunction analyzer*, J Comput. Chem., **33**, 580, (2012).

[33] R. S. Mulliken, *Electronic population analysis on LCAO-MO molecular wave functions*, J Chem. Phys., **23**, 1833, (1955).

[34] F. L. Hirshfeld, *XVII. Spatial Partitioning of Charge Density*, Isr. J Chem., **16**, 198, (1977).

[35] F. L. Hirshfeld, *Bonded-atom fragments for describing molecular charge densities*, Theor. Chim. Acta., **44**, 129, (1977).

[36] T. Lu, F. Chen, *Atomic dipole moment corrected Hirshfeld population method*, J Theor. Comput. Chem., **11**, 163, (2012).

[37] T. Lu, et al., *A Multifunctional Wavefunction Analyzer (Multiwfn)*, Software manual, **7**, 1, (2020).

[38] W. Humphrey, A. Dalke, K. Schulten, *VMD: Visual molecular dynamics*, J Mol. Graph., **14**, 33, (1996).

[39] S. M. Morton, L. Jensen, *Understanding the molecule-surface chemical coupling in SERS*, J Am. Chem. Soc., **131**, 4090, (2009).

[40] A. Becke, *The Quantum Theory of Atoms in Molecules-From Solid State to DNA and Drug Design*, John Wiley & Sons, 2007.

[41] D. Cremer, E. Kraka, *Chemical Bonds without Bonding Electron Density does the Difference Electron-Density Analysis Suffice for a Description of the Chemical Bond*, Angewandte Chemie International Edition in English, **23**, 627, (1984).

[42] C. Gatti, *Chemical bonding in crystals: new directions*, Zeitschrift für Kristallographie-Crystalline Materials, **220**, 399, (2005).

[43] H. Yang, P. Boulet, M. C. Record, *A rapid method for analyzing the chemical bond from energy densities calculations at the bond critical point*, Computational and Theor. Chem., **1178**, 112784, (2020).

[44] R. Pino-Rios, et al., *Orbital-weighted dual descriptor for the study of local reactivity of systems with (quasi-) degenerate states*, J. Phys. Chem. A, **123**, 10556, (2019).

[45] J. Menéndez, J. B. Page, *Vibrational spectroscopy of C60*, Light Scattering in Solids VIII, **76**, 27, (2006).

[46] Arizona State University, *The vibrational modes of buckminsterfullerene C60.*

[47] D. E. Weeks, W. G. Harter, *Rotation-vibration spectra of icosahedral molecules. II. Icosahedral symmetry, vibrational eigenfrequencies, and normal modes of buckminsterfullerene*, J Chem. Phys., **90**, 4744, (1989).

[48] H. Kuzmany, et al., *Raman spectroscopy of fullerenes and fullerene-nanotube composites*, Philosophical Transactions of the Royal Society A: Mathematical, Physical and Engineering Sciences, **362**, 2375, (2004).

[49] V. Schettino, et al., *The vibrational spectrum of fullerene C60*, J. Phys. Chem. A, **105**, 11192, (2001).

[50] S. M. Morton, L. Jensen, *Understanding the molecule surface chemical coupling in SERS*, J. Am. Chem. Soc., **131**, 4090, (2009).

[51] L. Zhao, L. Jensen, G. C. Schatz, *Pyridine-Ag20 cluster: A model system for studying surface-enhanced Raman scattering*, J Am. Chem. Soc., **128**, 2911, (2006).